Report on a problem studied at the Canadian Math-in-Medicine Study Group Toronto 2009
< http://www.maths-in-medicine.org/canada/2009/tumor-classification/ >

Proceedings of the OCCAM–Fields–MITACS Biomedical Problem Solving Workshop, 2009

Constitutive Models for Tumour Classification

Problem Presenter: Corina S. Drapaca (Pennsylvania State University)

Contributors: D. Aruliah (UOIT), R.D. Donaldson (Simon Fraser University), C.S. Drapaca (Pennsylvania State University), G. Lewis (UOIT), A. Sanchez (University of Waterloo), V. Takeva-Volkov (UOIT)

Report prepared by: D. Aruliah, R.D. Donaldson, C.S. Drapaca[1] and A. Sanchez

Abstract. The aim of this paper is to formulate new mathematical models that will be able to differentiate not only between normal and abnormal tissues, but, more importantly, between benign and malignant tumours. We present preliminary results of a tri-phasic model and numerical simulations of the effect of cellular adhesion forces on the mechanical properties of biological tissues.

1 Introduction

Diagnostic radiology is an exciting and rapidly expanding multi-disciplinary field of clinical medicine which links medicine to science and engineering. It enables noninvasive imaging and investigation of structure and function of the human body, and a unique insight into disease processes *in vivo*. One such imaging technique, called Magnetic Resonance Elastography (MRE), is used to measure the elasticity of biological tissues subject to mechanical stress [8, 9]. The resulting strains are measured using magnetic resonance imaging and the related elastic modulus is computed from models of tissue mechanics. The elastic modulus contains important information about the pathology of the imaged tissues. Thus, MRE can help in tumour detection, determination of characteristics of disease, and in assessment of rehabilitation.

It was noticed experimentally that most biological tissues have incompressible viscoelastic features: they have a certain amount of rigidity that is characteristic of solid bodies, but, at the same time, they flow and dissipate energy by frictional losses as viscous fluids do [3, 4]. The incompressibility assumption for soft tissues is based on the fact that most tissues are made primarily of water. In addition, since the displacements in MRE are very small (on the order of microns), a linear constitutive law is usually assumed. However, despite the richness of the data set, the variety of processing techniques and the simplifications made

[1] csd12@psu.edu

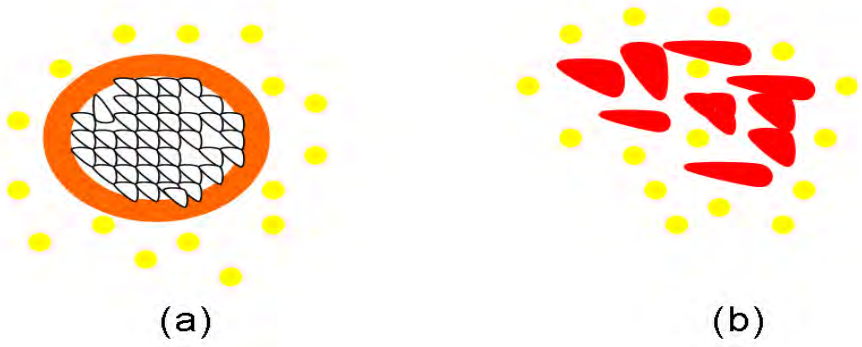

Figure 1.1 (a) Benign tumour: the fibrous connective tissue capsule (orange) separates the inside benign cells (black boundaries) from the outside normal cells (yellow). (b) Malignant tumour: the irregularly-shaped cancer cells (red boundaries) are anisotropic and non-localized.

in the biomechanical model, it remains a challenge to extract accurate results at high resolution in complex, heterogeneous tissues from the intrinsically noisy data. Therefore, any improvement in the MRE data processing with the help of biomechanics and computational methods will be of significant importance to modern medicine.

The aim of this paper is to formulate new mathematical models that will be able to differentiate not only between normal and abnormal tissues, but, more importantly, between benign (not cancerous) and malignant (cancerous) tumours. As it can be seen in Figure 1.1, benign tumours are localized, self-contained (encapsulated), with smooth boundaries, and tend to be more isotropic. On the other hand, malignant tumours are not localized, not self-contained, have irregular boundaries, and are anisotropic. Recent advancements in molecular biology [2] show that the cell-cell and cell-extracellular matrix adhesion forces play an important role in the localization of the tumours, with malignant tumours having a much poorer adhesion to the surroundings than benign tumours. It is important to notice that the cell-cell adhesions are rearranged dynamically during tissue development and tumour metastasis but the few existing mathematical models of the cell-cell adhesions are all static models. The modeling of the adhesion forces in normal tissues and tumours is still an open problem in mathematical biology.

In order for the MRE method to correctly classify the tumours of a given tissue as benign or malignant, the mathematical models of these two classes of tumours need to incorporate the differences between them. In the present paper we focus on mathematical models that incorporate information about microstructure and cellular adhesion forces. We pursued the following three approaches: (i) the simulation of the time-harmonic linear elastic models to examine coarse scale effects and adhesion properties, (ii) the investigation of a tri-phasic model, with the intent of upscaling this model to determine effects of electro-mechanical coupling between cells, and (iii) the upscaling of a simple cell model as a framework for studying interface conditions at malignant cells. The model used in simulation (i) is inspired by the dynamic MRE method where shear periodic forces are applied on the tissue [7].

2 Preliminary qualitative experiments

As a first step in developing a constitutive model that distinguishes benign and malignant cells, we consider a simple model of elastic waves propagating through inhomogeneous media. We start with a simple scalar PDE model (2.1) of transverse periodic waves propagating through an inhomogeneous, almost incompressible, linearly elastic tissue:

$$\frac{\partial^2 u}{\partial t^2} - \operatorname{div}\left(\mu(x,y)\nabla u\right) = 0, \qquad (x,y) \in \left(-\frac{1}{2},\frac{1}{2}\right)^2, \tag{2.1a}$$

$$u\left(x,-\frac{1}{2}\right) = \cos(\omega t), \qquad x \in \left[-\frac{1}{2},\frac{1}{2}\right], \tag{2.1b}$$

$$\frac{\partial u}{\partial t} + \sqrt{\mu}\frac{\partial u}{\partial n} = 0, \qquad x = \pm\frac{1}{2},\ y = \frac{1}{2}. \tag{2.1c}$$

The quantity u is the transverse displacement due to propagation of elastic waves and the quantity $\mu(x,y)$ is one of the Lamé coefficients, and n is the outward unit normal. Based on the fact that longitudinal waves propagate at much higher speeds than shear waves through biological tissues, we neglected any longitudinal effects. The boundary condition (2.1b) is the periodic force acting on the top of the domain that causes the transverse waves. The boundary condition (2.1c) is an absorbing (Sommerfeld) boundary condition to prevent reflection of waves. We generate simple finite-difference solutions of this wave equation to help us distinguish useful modelling criteria. We experiment with a simple geometry (a large tumour as in Figure 2.3) and a more complicated one (a cluster of smaller tumour cells as in Figure 2.4).

We assume that the motion within the tissue is time-periodic with a frequency equal to that of the forcing oscillations, ω. This allows the system (2.1) to be transformed into the frequency domain:

$$\omega^2 U + \operatorname{div}\left(\mu\nabla U\right) = 0, \qquad (x,y) \in \left(-\frac{1}{2},\frac{1}{2}\right) \times \left(-\frac{1}{2},\frac{1}{2}\right), \tag{2.2a}$$

$$U = 1, \qquad y = -\frac{1}{2}, \tag{2.2b}$$

$$\sqrt{\mu}\frac{\partial U}{\partial n} + \imath\omega U = 0, \qquad x = \pm\frac{1}{2},\ y = \frac{1}{2}, \tag{2.2c}$$

where U is the Fourier transformed displacement field at frequency ω.

The Sommerfeld condition (2.2c) introduces artifacts along the edges when waves are not traveling perpendicularly to the boundary. To combat this, the simulations were performed on a larger domain and then trimmed to remove the artifact. This effect is shown in Figure 2.1. Since most of the artifact is removed by trimming in this extreme case when waves are traveling parallel to the boundary, it is expected that this procedure will perform adequately when inclusions are introduced that deflect the travelling waves.

The system (2.2) was discretized on a rectangular grid, and converted into the following matrix problem:

$$L\widehat{U} = R, \tag{2.3}$$

where $\widehat{U}$ is a vectorized version of the displacement field, and L is a sparse matrix representing the discrete version of the left-hand operator with right-hand terms R from System (2.2). This was solved in MATLAB using the backslash operator, which implements a

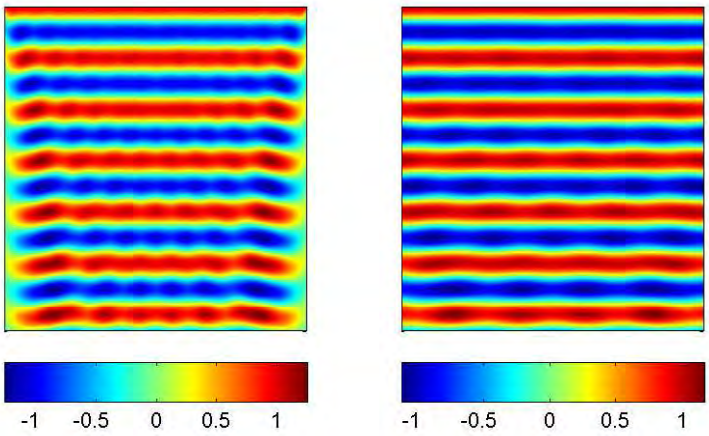

Figure 2.1 Left: Expanded domain with Sommerfeld conditions applied on the left, right and bottom sides. Right: trimmed domain to remove artifacts caused by the Sommerfeld conditions.

Table 2.1 Simulation Parameters

Grid Size	500×500 points
ω	100 Hz
$\mu_{\text{background}}$	250
$\mu_{\text{inclusion}}$	750

modified Sparse Cholesky Factorization method. The real component of the solution then represents the displacement field at time $t = 0$.

The lengths of the domain were scaled to be a unit square. The background stiffness of the material was then scaled to admit six full wavelengths, which corresponds to experiments performed on agar-agar gels in the MRE Lab at Mayo Clinic. The shear modulus for tumourous regions was set to three times that of the background to agree with the agar-agar experiments. Simulation parameters are summarized in Table 2.1.

Recall that benign tumours tend to adhere well to the surrounding normal tissue as compared to malignant tumours. Thus, for the full-adhesion simulations of benign tumours, we assume that there is a smooth, continuous transition between the background and tumour tissues. While the waves in Figure 2.3 change their wavelengths when passing through the stiffer tumourous regions (for reference see Figure 2.2 for the case without an inclusion), the waves in Figure 2.4 penetrate between the cluster of smaller tumours without a significant change of wavelengths. That is, there is a higher chance that the latter case will avoid detection when using the MRE technique.

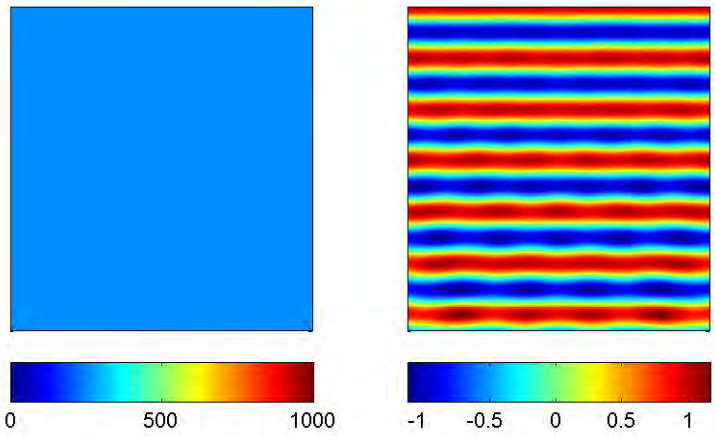

Figure 2.2 Propagation of elastic waves with no inclusions.

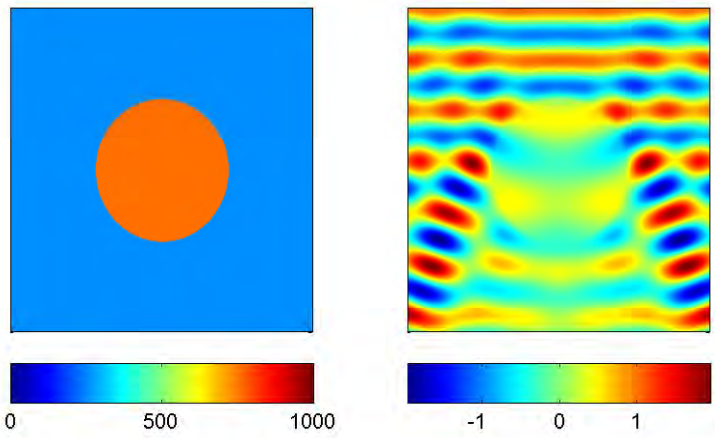

Figure 2.3 Propagation of elastic waves through a large tumour with perfect adhesion.

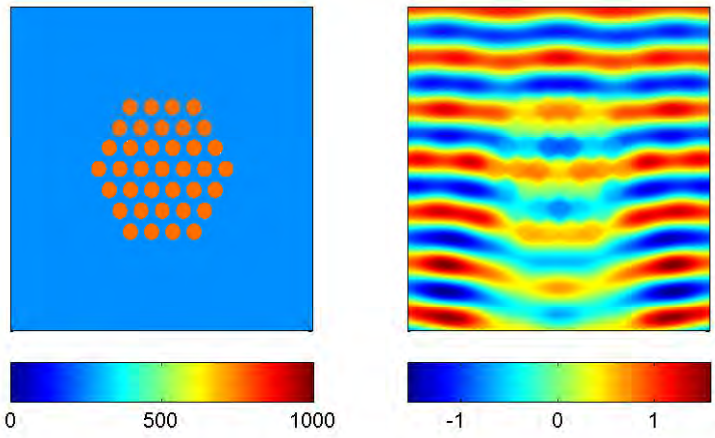

Figure 2.4 Propagation of elastic waves through a diffuse tumour with perfect adhesion.

To simulate a no adhesion property for malignant tumours, we impose a zero Neumann condition on the tumour-background tissue interface. To reduce complexity, normal derivatives along the interface were estimated using a first-order finite difference scheme. Because of this zero Neumann condition, the tumour regions are not affected by motions in the background material as seen in Figures 2.5 and 2.6.

In order to account for adhesive effects more realistically, we propose the following improved interface conditions to model cellular adhesions:

$$\mu \left[\frac{\partial U}{\partial n} \right]_{-}^{+} = \alpha [U]_{-}^{+}, \tag{2.4}$$

$$\mu \left[\frac{\partial U}{\partial \tau} \right]_{-}^{+} = 0, \tag{2.5}$$

where '+' indicates values in the background region, '−' indicates the tumour region, n is the normal direction at the interface from background to tumour, τ is the tangential direction, and α is an experimental jump parameter. Interface derivatives were estimated using first-order finite differencing. With this jump condition, points along the interface between background and tumour tissue must be repeated in $\widehat{U}$ in order to admit the two values U_+ and U_- at each interface point. Results are presented in Figure 2.7.

These preliminary experiments support the conjecture that adhesion effects can be observed in the measured displacement field and hence motivate a deeper exploration of multiscaling models that incorporate them.

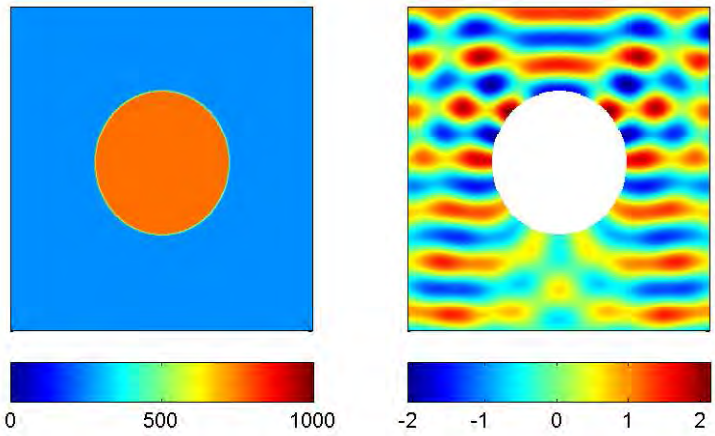

Figure 2.5 Propagation of elastic waves through a large tumour with no adhesion.

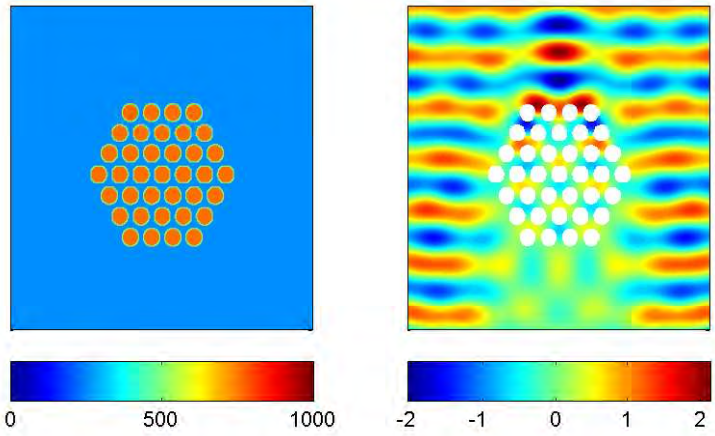

Figure 2.6 Propagation of elastic waves through a diffuse tumour with no adhesion.

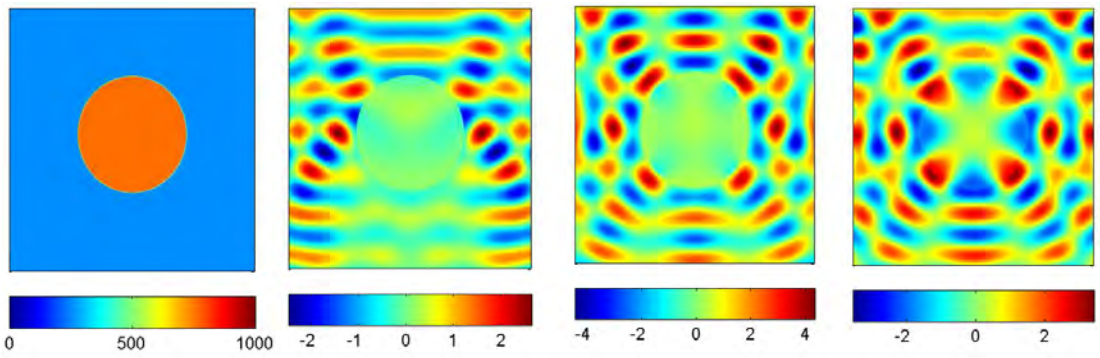

Figure 2.7 From left to right: $\alpha = 0$ (second image), $\alpha = 10^6$ (third image), and continuous boundary $U_- = U_+$ ($\alpha = \infty$) (forth image)

.

3 A tri-phasic model

Inspired by [12], we assume that a biological tissue is a mixture of an intrinsically incompressible, isotropic, porous-permeable-charged linear elastic solid phase containing the extracellular matrix and the (linear viscoelastic) solid cells, an intrinsically incompressible, isotropic, Newtonian viscous fluid phase containing the interstitial fluid, and an ion phase with, for now, two monovalent ion species: anion (-) and cation (+). The solid phase and the ion phase are electrically charged, while the fluid phase and the tissue as a whole are electrically neutral.

The constitutive equations are [5, 12]:

$$\sigma = -pI + \lambda_s eI + 2\mu_s \epsilon, \tag{3.1}$$

$$\mu^w = \mu_0^w + [p - RT(c^+ + c^-)\Phi + B_w e]/\rho^w, \tag{3.2}$$

$$\mu^+ = \mu_0^+ + (RT/M_+)\ln(\gamma_+ c^+) + F_c\psi/M_+, \tag{3.3}$$

$$\mu^- = \mu_0^- + (RT/M_-)\ln(\gamma_- c^-) - F_c\psi/M_-, \tag{3.4}$$

where the first equation is Hooke's law for the linear elastic phase, and the last equations are the constitutive equations for the fluid phase and the ion phase. We have denoted by p the fluid pressure, σ the stress tensor in the elastic solid, ϵ the strain tensor in the elastic solid with $e = \mathrm{tr}(\epsilon)$ λ_s, μ_s the Lamé coefficients which depend on solid volume fraction and ion concentrations c^+, c^-, R is the universal gas constant, T is the absolute temperature, B_w is a coupling coefficient, μ^w is the chemical potential of the fluid phase, μ_0^w is the reference chemical potential of the fluid, Φ is the osmotic coefficient, ρ^w is the true mass density of the fluid, ψ is the electric potential, γ_+, γ_- are the activity potential coefficients, μ^+, μ^- are the electro-chemical potentials of the ion species with μ_0^+, μ_0^- the corresponding reference electro-chemical potentials, M_+, M_- are the molar weights of the ionic species, and F_c is the Faraday constant.

The governing equations are:

$$\operatorname{div}\sigma = \rho^s \frac{\partial \mathbf{v}^s}{\partial t}, \tag{3.5}$$

$$\operatorname{div}\mathbf{v}^s + \operatorname{div}\mathbf{J}^w = 0, \tag{3.6}$$

$$\frac{\partial(\phi^w c^+)}{\partial t} + \operatorname{div}\mathbf{J}^+ + \operatorname{div}(\phi^w c^+ \mathbf{v}^s) = 0, \tag{3.7}$$

$$\frac{\partial(\phi^w c^-)}{\partial t} + \operatorname{div}\mathbf{J}^- + \operatorname{div}(\phi^w c^- \mathbf{v}^s) = 0, \tag{3.8}$$

where ϕ^w is the porosity of the tissue and the water and ion fluxes relative to the solid phase are given by:

$$\mathbf{J}^w = \phi^w(\mathbf{v}^w - \mathbf{v}^s), \tag{3.9}$$

$$\mathbf{J}^+ = \phi^w c^+(\mathbf{v}^+ - \mathbf{v}^s), \tag{3.10}$$

$$\mathbf{J}^- = \phi^w c^-(\mathbf{v}^- - \mathbf{v}^s), \tag{3.11}$$

with $\mathbf{v}^s, \mathbf{v}^w, \mathbf{v}^+, \mathbf{v}^-$ the velocities of the corresponding phases. The governing equations need to be solved for the solid displacement and the water and ion fluxes. The boundary conditions are continuity of these unknown quantities across the boundaries between phases. It is important to notice that the continuity equations of the ions will need to be changed such that they model abnormal diffusion processes happening in a tissue when tumours appear and start to grow. We will address these modeling issues in our future work.

We assume further that a biological tissue is locally homogeneous at the macroscopic scale and its microstructure is made of periodic pores. Each electroneutral pore is saturated with the same amount of each of the three phases. The upscaling homogenization must be done in both spatial and temporal scales, since mechano-chemical processes at the micro-scale are faster than those at the macro-scale. For simplicity, we can take the Laplace transform of the governing equations and do only the homogenization in space for the Laplace transformed quantities. We introduce the small parameter $\alpha = x/X << 1$ with x the pore length scale, and X the macroscopic scale length, and assume that

$$f(x, X; \alpha) = f_0(x, X) + \alpha f_1(x, X) + \alpha^2 f_2(x, X) + \dots,$$

where f is any of the Laplace transforms of $\mathbf{u}^s, \mathbf{J}^w, \mathbf{J}^+, \mathbf{J}^-$. Then the corresponding α^n-order boundary value problems, $n = 0, 1, 2, \dots$ will have to be solved. We plan to report on the solutions to these problems in our further publications.

4 Up-scaling a malignant tumour model

We assume that malignant tumours are characterised by their cells' dispersion, lack of adhesion, and higher stiffness relative to surrounding normal tissue. As such, we develop an elastomeric model for malignant tumours based on a two-scale homogenization, where our aim is to present the macro-scale effect rendered by elastomeric interactions of individual tumour cells with normal tissue at the micro-scale.

Figure 4.1 gives a schematic of the classical two-scale homogenization approach. We assume some small length scale ϵ, in our case representing the size of a single malignant tumour cell. Assuming a small-scale pattern, we solve a so-called cell- or *unit*-problem at this scale, and use the solution to the unit-problem to present a PDE model with average parameters, effective at scales much larger than ϵ. From the perspective of resolving malignant

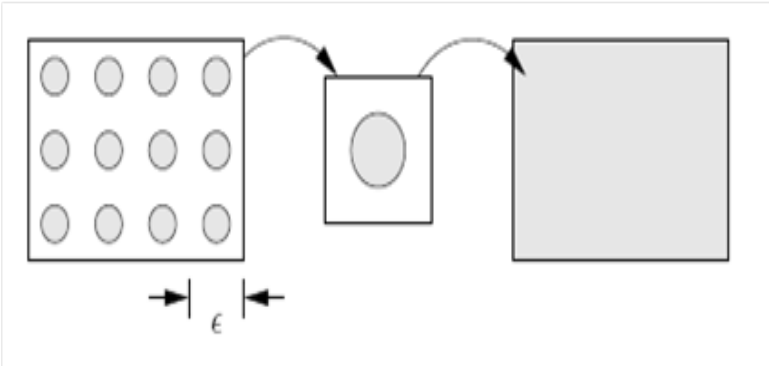

Figure 4.1 Schematic of up-scaling the dispersed malignant tumour model. From the periodic microscopic model at the left, we solve a pair of unit-problems [centre], and discover elastomeric parameters describing the average behaviour of the tissue at the large scale [right].

tumours, our expectation is that the parameters in the PDE up-scaled from this malignant cell model will differ greatly from those parameters representing a benign tumour.

Although we outline the development below, further details on two-scale homogenization for divergence-free systems can be found in several texts, see for example [6, 1].

4.1 Two-scale expansion. We examine a two-dimensional malignant cell model, whereupon the malignant cell is a circle in the centre of an ϵ-sized square, the remainder of the square representing healthy cells, see Figure 4.2. Our model is a PDE describing linear elastomerics in the time-harmonic case:

$$\begin{cases} \operatorname{div}(\mu\nabla u) + \omega^2\rho u = 0, & x \in \Omega, \\ \left[\mu\dfrac{\partial u}{\partial n}\right]^+_- = 0, & x \in \Lambda, \\ [u]^+_- = 0, & x \in \Lambda, \end{cases} \tag{4.1}$$

In our setting, we recall that only the second of the Lamé parameters, μ, (also the shear modulus) appears, owing to the remarkable difference between shear and compression wave speeds, and our subsequent detection only of shear waves in tissue. Parameters ω and ρ are the driving frequency and tissue density, respectively, and the solution $u : \Omega \to \mathbb{C}$ is understood to be the complex amplitude of the time-harmonic wave over the domain Ω, representing the excited tissue. At Λ, the interface between the malignant cell and its healthy surroundings, we assign two boundary conditions. These conditions represent the strength of the attachment of the malignant cell to other tissue, understood in reality to be quite poor. The notation $[\cdot]^+_-$ represents the jump in the argument from one side of Λ to the other. The boundary conditions in (4.1) represent a cell that is well-attached to its

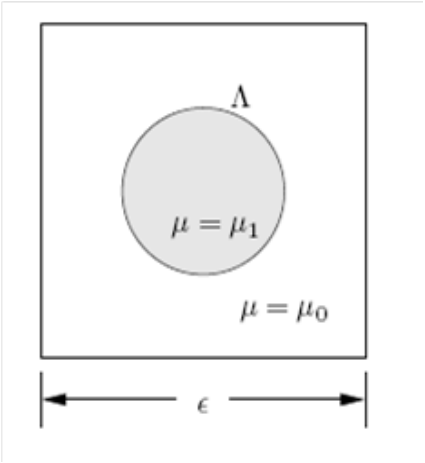

Figure 4.2 Unit cell geometry for up-scaling stiffness. The up-scaled stiffness parameter μ^* depends on the elastomeric stiffness parameter μ within and without of the malignant cell, as well as on the boundary conditions at the cell interface.

surroundings. In contrast, setting

$$\mu \frac{\partial u}{\partial n} = 0, \quad x \in \Lambda^+, \tag{4.2}$$

where Λ^+ represents the face of the boundary incident on the healthy cells, represents a malignant cell completely unadhered to the surrounding tissue. We examine these two extremes here, and suggest alternative boundary conditions which compromise between these two extremes at the end of this section. In any case, the up-scaled stiffness parameter μ^*, the effective stiffness at scales much larger than ϵ, will depend on the stiffness within and without of the malignant cell circle, as well as on the boundary conditions at the cell interface.

The up-scaling begins by assuming a two-scale solution,

$$u_\epsilon(x) = u(x, x/\epsilon) = u(x, y) \sim u_0 + \epsilon u_1 + \epsilon^2 u_2 + \ldots, \tag{4.3}$$

where u_ϵ is periodic in y, based on the observation that the shear modulus $\mu = \mu(x/\epsilon) = \mu(y)$. We refer to our ϵ-domain as $\mathcal{Y}$, which has unit area, and over which we have periodic boundary conditions. Applying this expansion to our model (4.1), we have

$$\epsilon^{-2} \left[\mathrm{div}_y(\mu \nabla_y u_0)\right] \tag{4.4}$$

$$+ \epsilon^{-1} \left[\mathrm{div}_y(\mu(\nabla_x u_0 + \nabla_y u_1)) + \mathrm{div}_x(\mu \nabla_y u_0)\right] \tag{4.5}$$

$$+ \epsilon^{0} \left[\mathrm{div}_x(\mu(\nabla_x u_0 + \nabla_y u_1)) + \mathrm{div}_y(\mu(\nabla_x u_1 + \nabla_y u_2)) + \rho\omega^2 u_0\right] \tag{4.6}$$

$$+ \mathcal{O}(\epsilon) = 0. \tag{4.7}$$

The $\mathcal{O}(\epsilon^{-2})$-term, combined with the periodic boundary conditions, gives $u_0 = u_0(x)$. Since $\nabla_y u_0 = 0$, the $\mathcal{O}(\epsilon^{-1})$ equation is

$$-\operatorname{div}_y(\mu \nabla_y u_1) = \operatorname{div}_y(\mu \nabla_x u_0(x)). \tag{4.8}$$

That is, the adjustment u_1 depends linearly on $u_0(x)$, and we can write

$$u_1(x,y) = \sum_{i=1}^{2} w_i \partial_{x_i} u_0, \tag{4.9}$$

where

$$-\operatorname{div}_y(\mu \nabla_y w_i) = \operatorname{div}_y(\mu \mathbf{e}_i) \tag{4.10}$$

together with boundary conditions on Λ form the *unit*-problem for the homogenization. $\mathbf{e}_i$ are unit basis vectors.

In the $\mathcal{O}(1)$-term in (4.7), we apply the $\mathcal{Y}$-periodicity of the solution, observing that

$$\int_{\mathcal{Y}} \operatorname{div}_y(\mu(\nabla_x u_1 + \nabla_y u_2)) = \int_{\partial \mathcal{Y}} \mu(\nabla_x u_1 + \nabla_y u_2)^T \widehat{n} = 0. \tag{4.11}$$

Thus, substituting $\nabla_x u_0(x) = \sum_{i=1}^{2} \mathbf{e}_i \partial_{x_i} u_0$, the linear dependence of u_1 on $\nabla_x u_0$ gives the $\mathcal{O}(1)$ equation

$$\operatorname{div}_x \left[\sum_{i=1}^{2} \left(\int_{\mathcal{Y}} \mu(\mathbf{e}_i + \nabla_y w_i) \right) \partial_{x_i} u_0 \right] + \rho \omega^2 u_0 = 0. \tag{4.12}$$

Finally, observing that as a weak solution to the unit-problem, the w_i satisfy

$$\int_{\mathcal{Y}} (\mathbf{e}_i + \nabla_y w_i)^T \mu \nabla_y w_j = 0, \tag{4.13}$$

we can rewrite (4.12) as

$$\operatorname{div}(\mu^* \nabla u_0) + \rho \omega^2 u_0 = 0, \tag{4.14}$$

where

$$\mu^*_{ij} = \int_{\mathcal{Y}} (\mathbf{e}_i + \nabla_y w_i)^T \mu (\mathbf{e}_j + \nabla_y w_j) \tag{4.15}$$

is the *up-scaled shear modulus*. The up-scaled modulus is clearly symmetric, and it is possible to show that provided $\mu(y) > 0$, then the operator resulting from μ^* is uniformly elliptic. Although it is common practise to normalize this integral by the volume of the unit cell, we have chosen $\operatorname{Vol}(\mathcal{Y}) = 1$ in this case.

Note that in general, even if μ is a scalar at the scale of the unit-problem, representing an isotropic shear modulus, expression (4.15) shows that it may not be scalar when up-scaled. In our setting, however, we have chosen the inclusion in our unit-problem to be circular. This avoids setting any preferred direction in our problem, and hence we expect our up-scaled shear modulus to be isotropic.

We have ignored any contribution of the Helmholtz term to the up-scaling calculation. It could happen, however, that for specific frequencies, $\omega \sim C/\epsilon$ for some constant C. In this setting, we would have to consider the effect of resonance at the scale of the unit problem, where the unit problem becomes an eigenvalue problem

$$-\operatorname{div}(\mu \nabla \phi) + (\rho \omega^2 - \lambda)\phi = 0. \tag{4.16}$$

See the lecture notes [10] for further details. Indeed, there is current research [13] in this area with respect to cancer treatments, where shear waves are tuned to resonate with and burst apart malignant cells. We do not pursue this case further here.

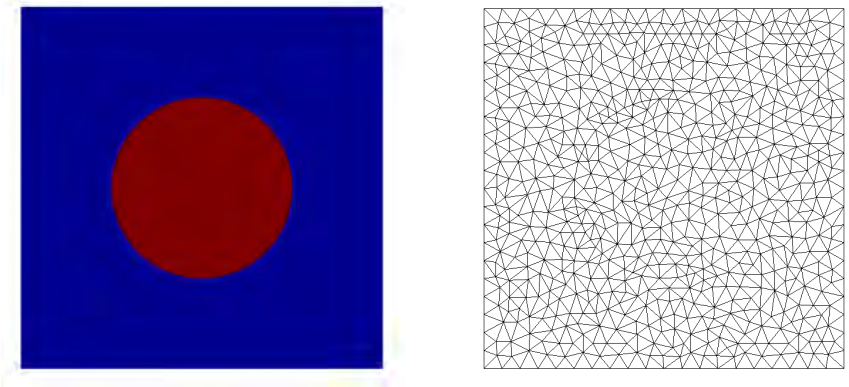

Figure 4.3 Numerical domain for the unit-problems. We discretize the unit-problem containing a tumour cell as a circular inclusion [left] using triangular finite elements [right].

4.2 Numerical results. We next examine two specific cases where we numerically solve unit-problems to up-scale the elastomeric effects of dispersed cells. In the first case, we solve

$$\begin{cases} -\operatorname{div}(\mu\nabla w_i) = \operatorname{div}(\mu\mathbf{e}_i), & x \in \mathcal{Y}, \\ \left[\mu\dfrac{\partial u}{\partial n}\right]_-^+ = 0, & x \in \Lambda, \\ [u]_-^+ = 0, & x \in \Lambda, \\ w_i \text{ are } \mathcal{Y}\text{-periodic.} \end{cases} \tag{4.17}$$

This unit-problem represents the case where the malignant cell is well-adhered to the surrounding tissue. We are aware that this case represents the opposite of our understanding of the biology, and we provide it for comparison with the following, more realistic model.

The second case we consider is

$$\begin{cases} -\operatorname{div}(\mu\nabla w_i) = \operatorname{div}(\mu\mathbf{e}_i), & x \in \mathcal{Y}, \\ \mu\dfrac{\partial u}{\partial n} = 0, & x \in \Lambda^+, \\ w_i \text{ are } \mathcal{Y}\text{-periodic.} \end{cases} \tag{4.18}$$

This represents a tumour cell completely unadhered to its surroundings. Although an extreme representation, it is straightforward to implement, and will suggest the effect boundary conditions present at the micro-scale can have on the up-scaled shear modulus.

In both cases, we choose $\mu = \mu_0 = 1$ in the healthy tissue, and $\mu = \mu_1 = 3$ in the malignant cell. A ratio of $\mu_0 : \mu_1 = 1 : 3$ is consistent with laboratory measurements of the shear modulus of healthy and cancerous tissue. Figure 4.3 shows the unit cell, discretized using triangular finite elements. We use Jonathan Shewchuk's Triangle program [11] to produce the triangulation.

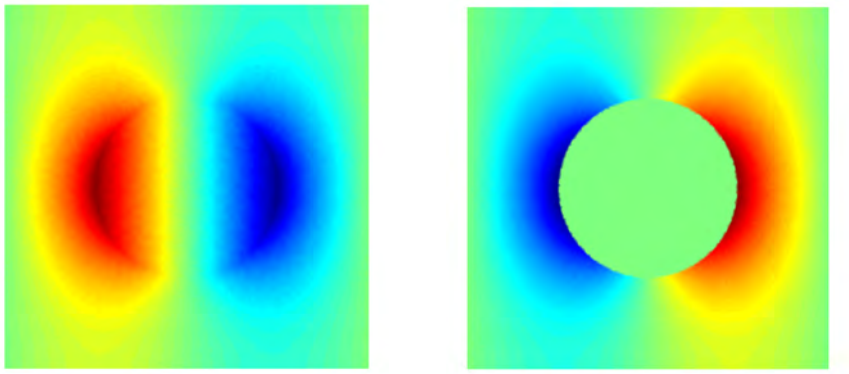

Figure 4.4 Well-adhered [left] and poorly-adhered [right] model unit-problems contrasted. Note that no information reaches the interior of the model cell in the case where the cell is poorly-adhered to its surroundings. Only the solutions to the x-direction unit-problem are shown: the y-direction solutions are simply these solutions rotated 90-degrees.

Table 4.1 Results of two contrasting unit problems. The shear modulus of the well-adhered cell is nearly double that of the case where the model cell is poorly-adhered to its surroundings.

Well-adhered problem (4.17)	$\mu^* = 1.22$
Poorly-adhered problem (4.18)	$\mu^* = 0.672$

Figure 4.4 contrasts the unit-problems for the well-adhered and poorly-adhered cases. (We show only the x-direction problems in each case. The y-direction problems are identical, only rotated 90-degrees.) The difference in the two problems is striking, showing the lack of flow of any information to the interior of the model cell in the case where the cell is poorly-adhered. This surely has an effect on the up-scaled shear modulus, as we see in the final results.

Table 4.1 summarizes our results, computing the integrals in (4.15) from the solutions in Figure 4.4. As anticipated by our choice of circular inclusion in the unit-problem, the up-scaled shear modulus is isotropic and we report only the diagonal values of (4.15). In summary, the case where the cell is poorly-adhered has a shear modulus half that of the well-adhered case. This indicates that the adherence of the malignant cells to the surrounding healthy cells can distinguish them from other cells, despite the small-scale dispersion of the malignant cells.

4.3 Further work. Following the homogenization framework, we propose several extensions to this up-scaling. The two most important modifications to the above model are to the boundary conditions at the malignant-normal cell interface, Λ, above, and to the choice of the shape of Λ.

Boundary conditions: We propose modeling the interface between normal and malignant cells according to the schematic of Figure 4.5. The schematic shows the cross-linking structures present between all cells, but in fewer number and stiffness between malignant cells and their surroundings. This reduced number of cross-links is precisely what reduces the adhesion between infected and normal cells, and affects a spring constant relating the normal stresses to the displacements of the cells, just as for one-dimensional Hooke's springs.

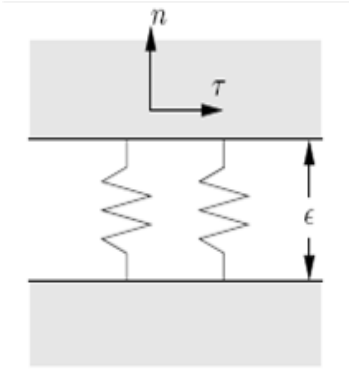

Figure 4.5 Model of the interface between normal and malignant cells. The density and strength of the cross-links, represented as wiggly lines, determines an effective spring constant relating normal stresses on each surface. Not shown is the visco-elastic effect of the fluid between the surfaces.

Furthermore, not shown in the schematic, the thin layer of pseudo-fluid between infected and normal cells gives a visco-elastic relationship between the two surfaces, such that the tangential stresses on the two surfaces are related to the relative strain rate of the surfaces. Combining the normal, n, and tangential τ, stress effects, we suggest the boundary conditions

$$\left[\mu \frac{\partial u}{\partial n}\right]_{-}^{+} = -\alpha \left[u\right]_{-}^{+}, \tag{4.19}$$

$$\left[\mu \frac{\partial u}{\partial \tau}\right]_{-}^{+} = -i\omega\beta \left[u\right]_{-}^{+}. \tag{4.20}$$

Note the imaginary number $i = \sqrt{-1}$ in the tangential condition, corresponding to a time-derivative for representing the strain rate.

The separation distance between cells, ϵ in Figure 4.5, is assumed sufficiently small that the constants α, β effectively summarize the adhesive properties of the malignant cell. Although the adhesion constants depend on properties of the normal-malignant interface we change the strain rate experimentally by tuning the driving frequency ω. Such tuning may allow us to take advantage of the particular adhesion coefficients in order to better detect malignant cells in the up-scaled shear stress.

Owing to the additional data structure required to represent this solution (two values for u are required on each mesh vertex on Λ) implementing this condition, and understanding its contribution to the up-scaled constitutive law, will have to remain future work for the time being.

Random cell orientation: Although the choice of a spherical malignant cell is realistic insofar as it predicts no anisotropy in the up-scaled constitutive law, malignant cells are more likely to be football-shaped, such as that depicted in Figure 4.6, with orientation or

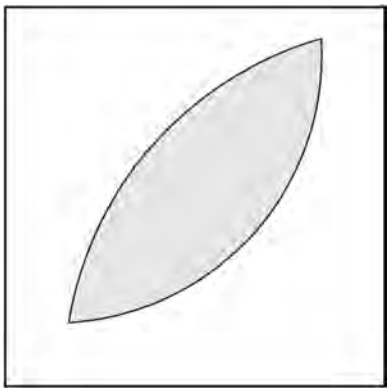

Figure 4.6 A more realistic malignant cell model shape. To avoid anisotropy in the up-scaled constitutive law, the orientation or other features of the cell geometry will have to be chosen in a random manner.

other features of the cell geometry being random. Such stochastic homogenization, where the aim is to compute the statistics of the constitutive law from the statistics of, in our case, the cell geometry, has been studied, and appears, for example, in lecture notes [10]. However, this is beyond the scope of our present investigation, and further study is required to see the effects of up-scaling a randomized unit problem.

5 Conclusion

The aim of this paper was to formulate new mathematical models that will be able to differentiate not only between normal and abnormal tissues, but, more importantly, between benign and malignant tumours. We pursued the following three approaches: (i) the simulation of the time-harmonic linear elastic models to examine coarse scale effects and adhesion properties, (ii) the investigation of a tri-phasic model, with the intent of upscaling this model to determine effects of electro-mechanical coupling between cells, and (iii) the upscaling of a simple cell model as a framework for studying interface conditions at malignant cells. Each of these approaches has opened exciting new directions of research that we plan to study in the future.

References

[1] G. Allaire, *Shape optimization by the homogenization method*, Springer-Verlag, 2002.

[2] A. Besser, U.S. Schwarz, *Coupling biochemistry and mechanics in cell adhesion: a model for inhomogeneous stress fiber contraction*, New J. Phys. **9** (2007), 1-27.

[3] F. A. Duck, *Physical Properties of Tissues- A Comprehensive Reference Book*, 6th edition, Sheffield, UK: Academic, 1990.

[4] Y.C. Fung, *Biomechanics - Mechanical Properties of Living Tissues*, 2nd edition, Springer, New York, 1993.

[5] W.Y. Gu, W.M. Lai and V.C. Mow, *A mixture theory for charged-hydrated soft tissues containing multi-electrolytes: passive transport and swelling behaviors*, J. Biomech. Engrg. **120** (1998), 169-180.

[6] U. Hornung, *Homogenization and porous media*, Springer-Verlag, 1997.

[7] A. Manduca, T.E. Oliphant, M.A. Dresner, J.L. Mahowald, S.A. Kruse, E. Amromin, J.P. Felmlee, J.F. Greenleaf and R.L. Ehman, *Magnetic resonance elastography: non-invasive mapping of tissue elasticity*, Med. Imag. Anal. **5** (2001), 237-254.

[8] R. Muthupillai, D.J. Lomas, P.J. Rossman, J.F. Greenleaf, A. Manduca and R.L. Ehman, *Magnetic resonance elastography by direct visualization of propagating acoustic strain waves*, Science **269** (1995), 1854-1857.

[9] R. Muthupillai, P.J Rossman, D.J. Lomas, J.F. Greenleaf, S.J. Riederer and R.L. Ehman, *Magnetic resonance imaging of transverse acoustic strain waves*, Magn. Reson. Med. **36** (1996), 266-274.

[10] A. Papanicolaou, *Diffusion in Random Media*, Lecture Notes, `ftp://math.stanford.edu/pub/papers/papanicolaou/make.pdf`, accessed June 2009.

[11] J. Shewchuk, *Triangle: A Two-Dimensional Quality Mesh Generator and Delaunay Triangulator*, Software, `http://www.cs.cmu.edu/ quake/triangle.html`, accessed June 2009.

[12] D.N. Sun, W.Y. Gu, X.E. Guo, W.M. Lai and V.C. Mow, *A mixed finite element formulation of triphasic mechano-electrochemical theory for charged, hydrated biological soft tissues*, Int. J. Numer. Meth. Engng. **45** (1999), 1375-1402.

[13] J. Tuszynski, private communication.